15th AIAA/CEAS Aeroacoustics Conference

Flow and Noise Simulation of the NASA Tandem Cylinder Experiment using OpenFOAM

Con J. Doolan*

The University of Adelaide, Adelaide, South Australia, 5005, Australia

The NASA Tandem Cylinder experiment has been simulated for the case where the cylinders were placed 3.7 diameters apart (center-to-center). This configuration allows vortex shedding to occur in the inter-gap region between the cylinders. Two-dimensional, unsteady Reynolds averaged Navier Stokes flow simulations were performed using the OpenFOAM open source code. Simulated mean and unsteady flow results compare well with published experimental data. The major discrepancies between numerical and experimental flow results can be attributed to neglecting the spanwise velocity component during simulation. Acoustic computations were made using two-dimensional flow data and a compact form of Curle's theory with spanwise and temporal statistical models that introduced random perturbations into the time-domain signals. The upper and lower frequency limits of the acoustic simulation method were selected using arguments based on acoustic compactness and an estimate of near-field acoustic effects. Acoustic simulation results compare well with experiment about the main tone. Further improvements are necessary to broaden tones at the harmonics.

I. Introduction

The noise generated by bluff body wake interference is important because it occurs in a wide variety of applications that include (but are not limited to) aircraft landing gear, industrial heat exchangers and in a myriad of architectural situations. Depending on bluff body separation geometry, the noise generated by wake interference can be more intense than that of a single bluff body, therefore it is important to have methodologies that enable engineers and scientists to understand the flow and noise generation physics as well as design new, quiet technology.

The arrangement of tandem, in-line cylinders is the most investigated form of wake interaction to be found in the literature. As originally classified by Zdravkovich,[1] tandem cylinder flows are classed as a problem in wake interference and the separation between the cylinders sets the type of wake interaction. Essentially, when the cylinders are close to one another, vortex shedding from the upstream cylinder has been found to be suppressed (defined as the sub-critical regime in this work). As the cylinder spacing is increased, a variety of flow modes are encountered (sometimes with hysterisis effects), with upstream shear layer reattachment occuring first on the downstream cylinder, followed by the re-estabishment of vortex shedding behind the upstream cylinder. Once this occurs, the impingement of the wake on the downstream body creates high amplitude unsteady forces and intense radiated noise (defined as the vortex-shedding regime). Hydrodynamic feedback between the cylinders synchronises their vortex shedding frequencies until the separation distance becomes very large. Most tandem cylinder studies have been performed at relatively low Reynolds number however; a recent experimental (and numerical) program has been performed at high Reynolds number (1.66×10^5) by NASA[2–4] (called the NASA Tandem Cylinder Experiment in this paper) that provides one of the most comprehensive data sets available for aeroacoustic simulation validation. Another important data set on tandem cylinder flow and noise can be found in the paper written by Hutcheson and Brooks.[5]

Our interest in the noise generated by tandem bluff bodies stems from recent experiments and simulations of the vortex wake interaction.[6] These results show that noise can either be intensified or reduced depending

*Senior Lecturer, School of Mechanical Engineering, Senior Member, AIAA.

on the phase difference between the aerodynamic forces acting on each body, provided assumptions concerning acoustic compactness are met. This is an interesting result, however, in order to explore it further and apply our ideas to more relevant engineering applications, validation of existing numerical methods needs to be performed.

There are a variety of methods to simulate flow and noise about bluff bodies. These include methods such as direct numerical simulation (DNS), Large Eddy Simulation (LES) or solving the Unsteady Reynolds Averaged Navier Stokes (URANS) equations. For Reynolds numbers of practical interest, the use of DNS is infeasible (due to current limitations in computational power) and some form of turbulence modelling is required. While LES is becoming popular, it is still computationally very expensive and most engineers will rely on two-dimensional URANS simulations to obtain flow results in a more timely manner. Usually, due to computational expense, flow is simulated in the acoustic near field only and often using an incompressible flow solver. Hence acoustic simulation must be performed in a second step using an acoustic analogy to transform the aerodynamic simulation results into far-field acoustic pressure.

There are relatively few simulations of the *flow and noise* generated by bluff body wake interference. There are some notable contributions at low Reynolds number with the DNS study by Inoue *et al.*[7] concerning interacting square cylinders particularly relevant. At Reynolds numbers of practical interest ($> 10^5$), only the simulations performed by NASA[2,8] and the wake interference study of Leclercq and Doolan[6] combine high Reynolds number interacting bluff body flow simulations and noise estimation. From these studies, only the NASA publications are concerned with cylindrical flows in both the sub-critical and vortex shedding regimes.

The NASA flow estimates were performed using a three-dimensional, compressible flow simulation about tandem cylinders and used a hybrid, zonal turbulence model that was active only in the boundary layer regions of the cylinders. Outside this region, no turbulence model was used, hence this was a type of Detached Eddy Simulation (DES), that used no specific sub-grid-scale model in the wake but relied instead on the dissipation of the numerical scheme to mimic turbulent energy transfer to the smallest scales. Noise was calculated using a Ffowcs Williams-Hawkings (FW-H) solver. Good predictions of the noise spectra were obtained for large cylinder spacing ($L/d = 3.7$, vortex shedding regime), however at small cylinder spacing ($L/d = 1.435$, sub-critical regime) predicted noise spectra only reproduce experimental trends and this is thought to be due to the flow simulation not calculating all the required flow dynamics in sufficient detail.

A two-dimensional URANS flow simulation of the NASA tandem cylinder experiment[3] has also been previously performed but with no noise prediction. It was shown that reasonable agreement with flow data was achieved but not all the wake dynamics could be captured in the two-dimensional simulation.

While not strictly bluff body wake interference, an important related study is the one performed by Casalino *et al.*[9] where the von Karman wake shed from a cylinder interacted with with a symmetrical airfoil whose leading edge was approximately 10 cylinder diameters downstream. In this work, a two-dimensional URANS simulation was performed and compared with experiment for $Re = 2.2 \times 10^4 - 1.37 \times 10^5$. Noise predictions were obtained using a FW-H solver with a statistical spanwise phase dispersion model to recreate three-dimensional effects along the span. Very good comparisons between numerical and experimental noise spectra were obtained.

From this survey, it appears that very few validation studies of tandem cylinder flow and noise simulations are currently available. Hence, any new studies in this area will shed light on the noise production mechanisms and on the methodologies used to predict them. Also, current engineering level predictions of noise are likely to use a two-dimensional URANS approach to estimate flow and noise, simply due to the reduced simulation time of these methods compared with three-dimensional LES/DES approaches. However, there are no tandem cylinder noise experimental comparisons available for two-dimensional URANS solutions to guide their accurate implementation.

This paper presents flow and noise results based on an incompressible, two-dimensional URANS simulation of the NASA tandem cylinder experiment in the vortex shedding regime ($L/d = 3.7$). The numerical results are compared with previously published experimental data.[2–4] The flow simulations were performed using the OpenFOAM[10,11] software package. This is open source software that is used and developed by an international user community. While extensively used for a wide variety of aeronautical and industrial problems, the use of this code in the field of aeroacoustics is limited. This work presents the first use of this code for calculating flow and noise from tandem cylinders at this Reynolds number. Noise was calculated using a statistical phase dispersion model, based on the previous work of Casalino and Jacob,[12] but modified to use a compact version of Curle's formulation[13] and to account for temporal decorrelation of the sectional

lift coefficents. This study is also intended as preliminary work for a future airframe noise benchmarking workshop that was proposed at the 14th AIAA/CEAS Aeroacoustics meeting.

Specifically, the aims of this paper are as follows:

1. To present a 2D URANS flow and noise simulation of the NASA tandem cylinder experiment using OpenFOAM and assess the accuracy of the flow results against published experimental data.

2. To present a statistical noise calculation method, use it to predict tandem cylinder noise and assess its performance against published experimental data.

The paper is organised as follows: Section I introduces the work that is intended to be presented, some background, the aims of the paper and identifies the new and significant aspects of this work. Section II summarises the numerical techniques developed for this work. Section III compares the aerodynamic simulation results with experimental data and Section IV will compare numerical and experimental acoustic results using the models developed in this work. Preliminary conclusions are outlined in Section V.

II. Numerical Method

A. Aerodynamic Simulation

The aerodynamic part of the simulation was performed using OpenFOAM,[10,11] an open source numerical simulation system. The flow domain consisted of two cylinders of diameter d separated by a distance $L = 3.7d$ (between centers). The cylinders were immersed in a freestream flow of velocity U_0. The Reynolds number was matched to the NASA tandem cylinder experiment with $Re = 1.66 \times 10^5$. The Mach number (used for acoustic simulations) was matched to the experiments obtained in the Quiet Flow Facility (QFF)[2] with $M = 0.1274$.

The simulation solved the incompressible unsteady Reynolds Averaged Navier Stokes (URANS) and continuity equations using the k-epsilon turbulence model. A second-order discretization method was used for the convective fluxes. A second-order centered scheme was used for the viscous terms and a second-order implicit time-stepping method was used to estimate the temporal terms.

Three orthogonal grids were used to investigate the flowfield. A summary of these grids are shown in Table 1. Also shown in Table 1 are the mean and root-mean-square (rms) lift coefficient values for the upstream and downstream cylinders and experimental results[4] for the drag coefficients on each cylinder. As grid resolution is increased, the force coefficients approach a converged result and for this reason, Grid 3 (205,508 nodes) is used for the remainder of the analysis in this paper. The drag coefficients for the upstream cylinder is too low when compared with experiment. This is due to the incorrect prediction of mean separation position on the cylinder surface. Much better predictions are obtained for the downstream cylinder. More detailed analysis of the mean and fluctuating flow are presented later in this paper.

Table 1. Summary of average results from three computational grids and comparison with experiment.

Case	Nodes	$\overline{C}_{D,up}$	$C'_{L,up}$	$\overline{C}_{D,down}$	$C'_{L,down}$
Grid 1	101,902	0.271	0.075	0.237	0.393
Grid 2	146,406	0.305	0.082	0.240	0.438
Grid 3	205,508	0.338	0.086	0.245	0.487
Experiment[4]	-	0.49-0.52	-	0.24-0.35	-

The topology of Grid 3 is shown in Fig. 1. On average, y^+ was maintained between 30 and 40 on both cylinders, making the use of turbulent wall functions necessary. A non-dimensional time-step of $\frac{\Delta t U_0}{d} = 0.0007$ was used and the Courant number was kept below 0.5 at all times. The flow became statistically stationary before a non-dimensional time of $\frac{tU_0}{d} = 180$ was reached and data sampling occurred over the time range $180 \leq \frac{tU_0}{d} \leq 550$ (approximately 114 vortex shedding cycles).

B. Acoustic Simulation

1. Curle's Theory

Due to the dimensions of the experiment and the acoustic wavelengths of interest, a compact acoustic analogy was used to determine the far-field sound pressure level from the numerical results. Based on a Mach number of $M = 0.1274$, it would be expected that a compact analogy would break down at a Strouhal number above $St = fd/U_0 = 7.84$ assuming a wavelength based on the cylinder diameter. All noise results are presented over a Strouhal number range $0.1 \leq St \leq 2$, hence the compact assumption is appropriate. Further, in this work, quadrupole sources of noise are neglected. This has been shown to be valid and accurate for flows of this type and Reynolds number.[2,6]

The acoustically compact form of Curle's equation[13] can be simplified to predict the acoustic far field generated at an observation point by a fluctuating point force $\tilde{F}$ applied on a compressible fluid that is initially at rest

$$4\pi c_0^2 \left(\rho(\tilde{x},t) - \rho_0\right) = -\frac{\partial}{\partial x_i}\left[\frac{F_i}{r}\right] = \frac{1}{c_0}\frac{x_i}{r^2}\left[\frac{\partial F_i}{\partial t}\right] \tag{1}$$

where F_i are the three vector components of the resulting force applied on the fluid, c_0 and ρ_0 are the speed of sound and the fluid density in the medium at rest. The observation point is $\tilde{x}$ measured with respect to the compact body (in this case, the centre of the cylinder). The distance between the body and the observation point is described by the distance r. The square brackets denote a value taken at the retarded time $\Theta = t - r/c_0$.

In the case of a harmonic force, $F_i(t) = \mathrm{Re}\left(F_i e^{-i\omega t}\right)$ and

$$4\pi c_0^2 \left(\rho(\tilde{x},t) - \rho_0\right) = -F_i \frac{i\omega}{c_0}\frac{x_i}{r}\frac{e^{-i\omega\Theta}}{r} \tag{2}$$

Hence, the compact prediction assumes that the noise is of dipolar nature whose magnitude is controlled by the fluctuating force magnitude. A URANS simulation can provide this information in a straightforward manner. However, it is well known that transient force data from these types of simulations are extremely tonal and tend to overestimate the vortex shedding frequency, and its harmonics, resulting in poor noise predictions. The reasons behind these deficiencies results from the two-dimensionality of the simulation and, to some extent, the nature of the turbulence model employed.[9] It is mainly due to the over-prediction of Reynolds stresses in the near wake artificially constraining the size of the re-circulation bubble formed immediately behind the bluff body.[14] Two-dimensional simulations also have no capacity to incorporate spanwise fluctuations in velocity. In reality, these fluctuations result in a spanwise variation in the vortex shedding phase that manifests itself as perturbations in surface pressure and a de-correlation of the phase of the section lift and drag coefficients. Unsteady, three-dimensional wake velocities also result in random, intermittent disturbances to the vortex shedding, that are due to near cylinder vortex dislocations.[15]

For an acoustically compact cylinder with finite span, Curle's equation can be modified to take into account a spanwise variation in phase of the section lift and drag forces,

$$4\pi c_0^2 \left(\rho(\tilde{x},t) - \rho_0\right) = \int_{-\eta/2}^{\eta/2} -\frac{1}{c_0}\frac{x_i(\eta)}{r(\eta)^2}\left[\frac{\partial F_i(\eta)}{\partial t}\right] \mathrm{d}\eta \tag{3}$$

$$= \int_{-\eta/2}^{\eta/2} -F_i(\eta)\frac{i\omega}{c_0}\frac{x_i(\eta)}{r(\eta)}\frac{e^{-i(\omega\Theta+\phi_\eta)}}{r(\eta)}\mathrm{d}\eta \tag{4}$$

where η is a spanwise coordinate non-dimensionalised by the span (zero is at the cylinder mid-span), $F_i(\eta)$ is the sectional force in the i direction, acting at the η spanwise coordinate, $r(\eta)$ is the distance to the observation point from the particular spanwise location and $x_i(\eta)$ are the point coordinates of the observation point referenced to the spanwise location on the cylinder. De-correlation of the noise occurs due to a random dispersion of the phase ϕ_η along the span. Hence, some aspects of a three-dimensional flow field can be incorporated into a two-dimensional URANS simulation if a statistically accurate representation of the spanwise phase distribution can be found.

In addition to the spanwise dispersion in phase, the random, intermittent nature of the transient surface pressure and sectional force coefficients needs to be taken into account. Above a Reynolds number of

$Re = 5000$, the nature of turbulent transition changes in the near wake. In this regime, transition begins in the shear layers with KH vorticies becoming unstable along with pairing and possibly splitting.[16] This results in strengthening of streamwise vorticity and large scale vortex dislocation in the near wake. The effect on surface pressure is the introduction of low frequency modulations, reminiscent of the frequency "beating" phenomenon when two tones of nearly the same frequency are superimposed. This phenomenon has been observed experimentally[15] and numerically[2,17] when three dimensional simulations are performed. However, these effects are not recreated in a two dimensional URANS simulation and need to be introduced in order to correctly recreate the spectral broadening observed in experiment. This is done in the present work using a separate pre-processing step where a temporally based statistical model is used to introduce transient disturbances in the sectional unsteady lift and drag coefficients.

2. Spatial Statistical Model

Recently, Casalino and Jacob[12] have developed an ad-hoc technique to overcome some of the problems associated with URANS solutions in noise prediction. It accounts for the three-dimensional nature of the flow by randomly dispersing the phase of surface pressure fluctuations across the span of a cylinder (or any other extruded two-dimensional shape) according to a statistical model based on an estimate of the spanwise coherence. The random phase is then used to perturb the retarded time of surface pressure fluctuations across the span, which are then used in an FW-H solver to calculate far-field noise.

In the present paper, this method is modified to use the compact form of Curle's equation (Eq. 1) and is applied to the tandem cylinder experiment. Following Casalino and Jacob,[12] random phase distributions are determined using a linear variance distribution (w) across the span

$$w(\eta) = 2w_{max}|\eta| \tag{5}$$

A linear variance distribution results in a Laplacian correlation coefficient, giving

$$w_{max} = 1/L_l \tag{6}$$

where L_l is Laplacian spanwise correlation length scale. Hence, the model describing the correlation coefficient $\rho(\eta)$ across the span is (for Laplacian statistics)

$$\rho(\eta) = \exp\left(-\frac{|\eta|}{L_l}\right) \tag{7}$$

Using the spanwise statistical model, a random dispersion in phase (ϕ_η) is created along the span of the cylinder.

The phase distribution is then used to modulate the retarded time used in Eq. 4

$$\Theta_\eta = \Theta + \frac{\phi_\eta}{2\pi}\frac{d}{U_0} \tag{8}$$

This procedure is equivalent to introducing a spanwise loss of coherency along the span of a cylinder. It is a convenient way of introducing some of the features of a three-dimensional flowfield to a noise calculation that uses a two-dimensional flow simulation.

3. Temporal Statistical Model

In addition to the spanwise decorrelation of the force, there are statistical features of the transient sectional force data that are not captured by the simulated URANS simulation. A new method is described below whose aim is to introduce random features into the near-tonal URANS unsteady sectional force or surface pressure signals so that they more closely approximate experiment. Norberg[15] provides an excellent summary of this seemingly random behaviour of surface pressure fluctuations observed in cylinder flows.

It is assumed that the true signal $y(t)$ is convoluted over a signal of time length T to the simulated signal $x(t)$ using an impulse response function $h(t)$

$$y(t) = \int_0^T h(\tau)x(t-\tau)\,d\tau \tag{9}$$

The autocorrelation function of the true signal is therefore

$$R_y(\tau) = \iint_0^T h(\tau_1)h(\tau_2)R_x(\tau + \tau_1 - \tau_2)\, d\tau_1\, d\tau_2 \tag{10}$$

where the autocorrelation function of the simulated signal is $R_x(t)$. Assuming the simulated signal is approximately tonal, i.e. $x(t) \approx \mathcal{A}e^{-i\omega t}$, its autocorrelation function will be tonal as well

$$R_x(t) \approx \mathcal{B}e^{-i\omega t} \tag{11}$$

The autocorrelation function of the true signal then becomes (with $\mathcal{B}$ a complex constant)

$$R_y(\tau) \approx \mathcal{B}e^{-i\omega\tau} \int_0^T h(\tau_1)e^{-i\omega\tau_1}\, d\tau_1 \int_0^T h(\tau_2)e^{i\omega\tau_2}\, d\tau_2 \tag{12}$$

If the impulse response function can be described as

$$h(t) = e^{-i\phi_\tau} \tag{13}$$

then the true signal can be considered as a composite of a number of original simulated signals, each with a randomly dispersed phase difference $\phi_\tau = \phi_\tau(\tau)$. Noting that the cross-spectral function between two identical tonal signals ($x(t)$ and $x'(t)$) separated by a phase ϕ_τ is

$$R_{xx'}(t) = \mathcal{B}'e^{-i\phi_\tau}e^{-i\omega t} \tag{14}$$

where $\mathcal{B}'$ is a constant. Using Eqs. 13 and 14, the autocorrelation function for the true signal (Eq. 12) is

$$R_y(\tau) \approx \mathcal{C}e^{-i\omega\tau} \int_0^T R_{xx'}(\tau_1)\, d\tau_1 \int_0^T R_{xx'}(-\tau_2)\, d\tau_2 \tag{15}$$

where $\mathcal{C}$ is a new constant formed from the transformation. Recalling that the correlation coefficient function is

$$\rho_t(\tau) = \frac{R_{xx'}(\tau)}{\sqrt{R_x(0)^2}} \tag{16}$$

The approximation of the true autocorrelation function becomes

$$R_y(\tau) \approx \mathcal{D}e^{-i\omega\tau} \int_0^T \rho_\tau(\tau_1)d\tau_1 \int_0^T \rho_\tau(-\tau_2)\, d\tau_2 \tag{17}$$

In the same manner as the spatial case,[12] it is assumed that the correlation coefficient can be distributed according to Laplacian statistics

$$\rho_\tau(\tau) = \exp\left(-\frac{\tau_t}{\tau_c}\right) \tag{18}$$

so that $\tau_t = \tau/T_t$ is the time delay normalised by the time base T_t and $\tau_c = \Delta t_c/T_t$ is a normalised time scale associated with the randomness of the time signal.

Taking the limit $T \to \infty$, the autocorrelation function becomes proportional to τ_c^2. Hence, the signal power (or rms) will be progressively reduced as the time signal becomes more decorrelated (provided that the mean remains zero). However, in the following simulations, the power of the simulated URANS signals are preserved through the statistical transformation, making the direct evaluation of the constant $\mathcal{D}$ not necessary (although it is certainly possible). Original signal power is preserved because it is found that URANS simulations tend to predict this quantity reasonably accurately with respect to experiment.

The temporal statistical model is implemented in a similar manner to the spanwise statistical model where a random dispersion of phase (ϕ_τ) is used to decorrelate the URANS signal in the time domain. Consistent with the spanwise model, Laplacian statistics are assumed however, Gaussian statistics could equally be applied. The Laplacian model calls for a linear distribution of variance over $0 \leq \tau_t \leq 1$

$$w_\tau(\tau_t) = w_{\tau,max}\tau_t \tag{19}$$

where $w_{\tau,max} = 1/\tau_c$. This variance distribution is used to generate a random dispersion of phase (ϕ_τ) over $0 \leq \tau_t \leq 1$ that modulates the retarded time of the URANS signal using

$$\Theta_\tau = \Theta + \frac{\phi_\tau}{2\pi}\frac{d}{U_0} \tag{20}$$

This modulation is performed as a pre-processing step before the spanwise decorrelation of the signals. Practically, 100 URANS unsteady force data records, each with a randomly dispersed phase, are used to create a single temporally decorrelated signal. Previous attempts to incorporate the same temporal physics have involved ad-hoc methods within the spanwise model itself (see Casalino and Jacob[12]).

4. Frequency Compensation

The experimental data has been shifted in frequency so that the main tone occurs at an identical Strouhal number to the URANS simulation. According to Curle's theory (Eq. 2), linear frequency scaling also necessitates a small scaling in amplitude. The frequency and amplitude were scaled according to

$$f_{shift} = f\frac{St_{\text{num}}}{St_{\text{exp}}} \tag{21}$$

$$\Delta\text{SPL(dB)} = 20\log_{10}\frac{St_{\text{num}}}{St_{\text{exp}}} \tag{22}$$

5. Near-Field Correction

In the experimental study,[2] the microphones were placed approximately one wavelength from the acoustic source. This microphone location is normally not considered to be a purely radiative acoustic field and will contain some near-field hydrodynamic effects. A model has been developed to investigate the level of near-field contamination and hence appropriateness of the compact Curle formulation used for acoustic analysis.

If it is assumed that the acoustic field is dipolar in nature (as in this case), then the complete relation for the pressure at distance r from a dipole source with strength F_i is[18]

$$p'(\tilde{x},t) = \frac{1}{4\pi c_0}\frac{x_i}{r^2}\left[\frac{\partial F_i}{\partial t} + \frac{c_0 F_i}{r}\right] \tag{23}$$

This equation differs from Curle's compact formulation in that it includes a near-field term, inversely proportional to the distance to the observer r. Using the original dipole formulation, a frequency dependent correction term can be calculated for the simulated acoustic spectra. Recalling that, for harmonic signals, $\frac{-1}{i\omega} = \int dt$ and the usual relationships for wavelength (λ), Strouhal and Mach numbers,

$$p'(\tilde{x},t) = \frac{1}{4\pi c_0}\frac{x_i}{r^2}\left[\frac{\partial F_i}{\partial t}\right]\left[1 - \frac{c_0}{i\omega r}\right] \tag{24}$$

$$= p'_{curle}\left[1 + \frac{i\lambda}{2\pi r}\right] \tag{25}$$

$$= p'_{curle}\left[1 + \frac{i}{2\pi StM(r/d)}\right] \tag{26}$$

An expression for an appropriate frequency dependent correction to be applied to the simulated spectra can now be derived

$$\text{SPL}_c\ \text{(dB)} = 20\log_{10}\sqrt{1 + \frac{1}{4\pi^2 St^2 M^2 (r/d)^2}} \tag{27}$$

Figure 2 plots the magnitude of the near-field dB correction for the position where microphone B was placed during the experimental campaign[2] and where acoustic simulations were performed. The microphone was placed at $r/d = 33.74$, which corresponds to approximately one wavelength at the frequency of the main

tone ($St = 0.232$). The correction required to take into account near-field effects is small at the fundamental frequency (0.15 dB) and becomes vanishingly small as the Strouhal number (frequency) increases. Acoustic simulations are limited to $0.1 \leq St \leq 2$, therefore the maximum required near-field correction occurs at $St = 0.1$ and is 0.56 dB. If simulations were performed at lower frequency, then near field effects become more prominent and should be included in the simulation (as indicated in the figure). In this paper, near field effects are shown to be small and no corrections are made to the acoustic simulations made using the compact form of Curle's theory.

Hence, the acoustic simulation method used in this paper has a lower frequency limit imposed by microphone placement and near field effects. The simulation method also has an upper frequency limit imposed by assumptions of acoustic compactness. The above discussion and analysis justifies the choice of $0.1 \leq St \leq 2$ as a valid frequency range for the presented acoustic simulation.

III. Aerodynamic Results

A. Mean Flow

1. Mean Velocity

A comparison between computed and experimental streamlines[4] is shown in Fig. 3. The experimental results show an asymmetry which is thought to be due very small flow angularities. The recirculation bubble behind the upstream cylinder is comparable in size with the experiments, however the simulated recirculation bubble is much larger than experiments for the downstream cylinder.

Comparisons of the numerical and experimental[3] (PIV) mean streamwise velocity fields in the cylinder gap region are shown in Figs. 4. The URANS result shows a recirculation bubble size that is comparable with experimental PIV. The simulated velocity immediately downstream is significantly higher than experiment, resulting in a high velocity gradient when approaching the downstream cylinder stagnation point.

Figure 5 compares the URANS mean streamwise velocity along the centreline ($y = 0$) with experimental values obtained from the NASA Basic Aerodynamic Research Tunnel (BART) facility.[2] This result confirms that the upstream cylinder recirculation bubble is reasonably predicted. However, mean velocity downstream of $x/d = 1.7$ is over predicted, resulting from too high a entrainment rate of free-stream flow into the gap region. This results in an over prediction of the mean stagnation region surface pressure on the downstream cylinder (see below). The reasons for this behaviour in the URANS simulation is most probably linked to the incorrect prediction of Reynolds stress, distorting the recirculation bubble shape. In the tandem cylinder case, this effect has not changed the bubble length, but has constrained its width. A similar effect is distorting the downstream cylinder recirculation bubble as well.

Experimental and numerical mean vertical velocities in the cylinder gap region are compared in Fig. 6. Reasonable comparison is shown between the PIV and URANS results. Good comparisons between experimental PIV and numerical URANS results are observed for the time averaged streamwise velocity fluctuation, as shown in Fig. 7. The simulated fluctuation intensity is greater about the downstream cylinder, when compared with experiment.

2. Mean Surface Pressure

Computed (URANS) mean surface pressures about the upstream and downstream cylinders are shown in Fig. 8. Compared against the URANS data are experimental results[2] from both the BART and QFF facilities.

For the upstream cylinder, the overall comparison is good. The prediction of the separation points is slightly further around the cylinder than in experiment. The minimum pressure is over-predicted, however, the experiment is also perturbed by turbulence trips and a slight flow angularity. Computed base pressure matches better with the QFF experimental results and this may be due to the lack of upper and lower side-walls in this test, better approximating the boundary conditions used in the computation.

For the downstream cylinder, there is again good overall agreement between computation and experiment. There is poor agreement at the stagnation region and this is due to an over estimation of the mean streamwise flow velocity in the simulation. The effect of flow angularity is more evident in the experimental results. The QFF data match the URANS data more closely in the base region.

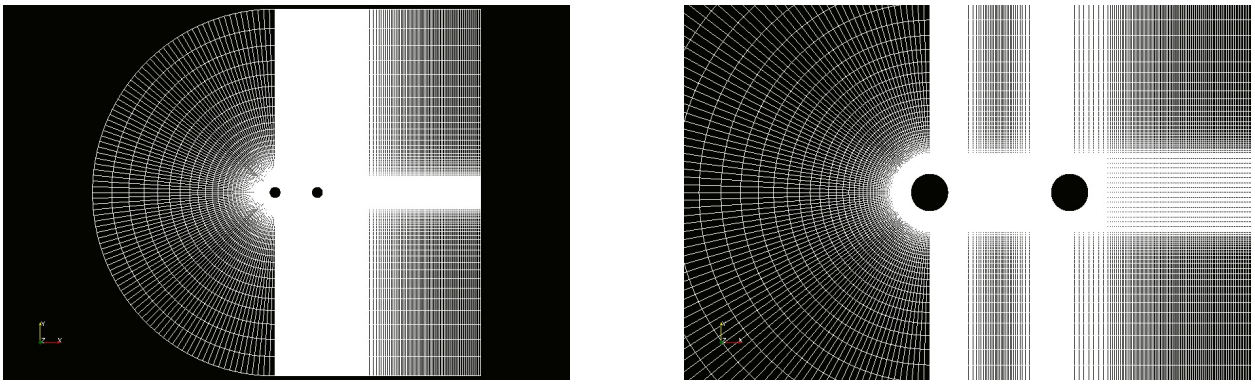

(a) Full domain (b) Region about cylinders

Figure 1. Computational Grid

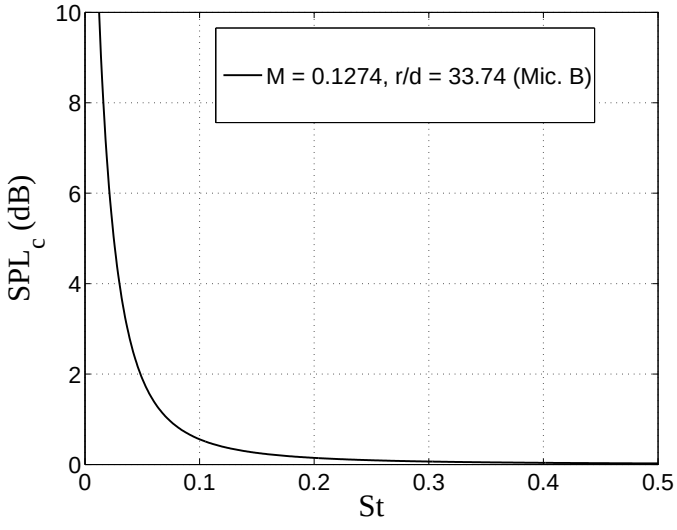

Figure 2. Near-field correction for the position of microphone B in the QFF experiments[2]

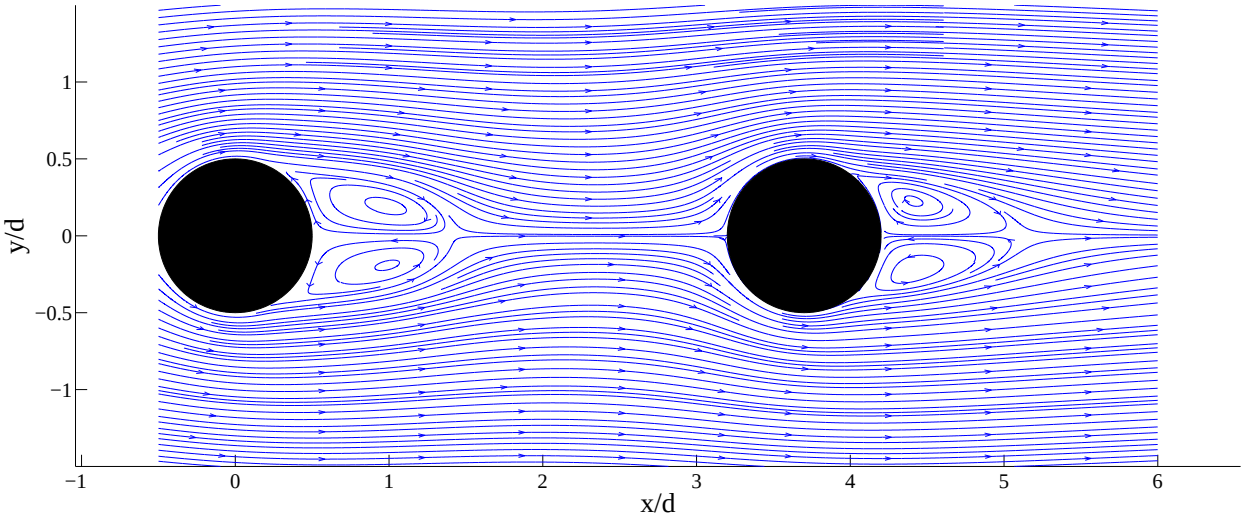

(a) URANS

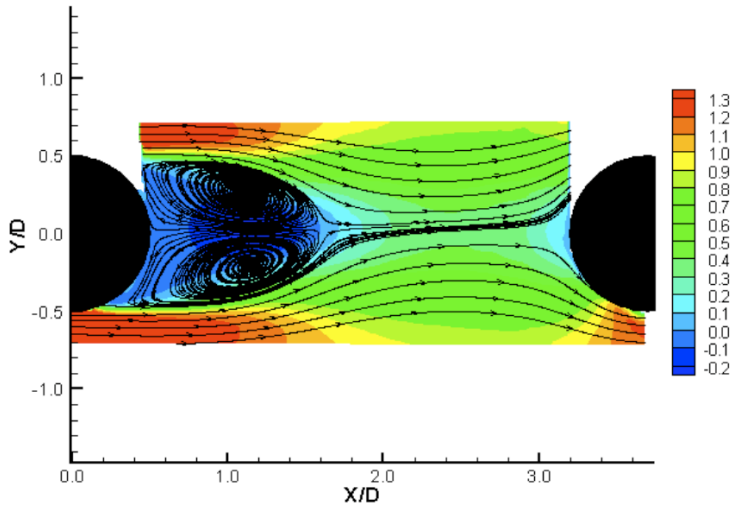

(b) NASA PIV data,[4] gap region

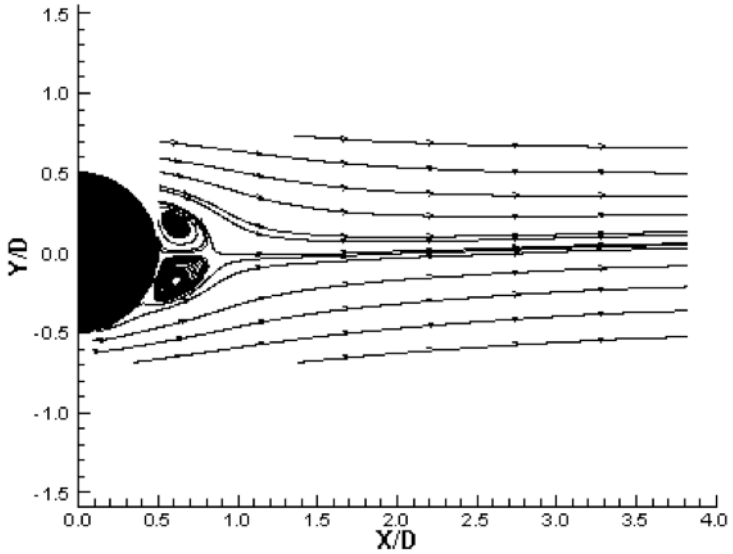

(c) NASA data,[4] near wake region

Figure 3. Streamlines

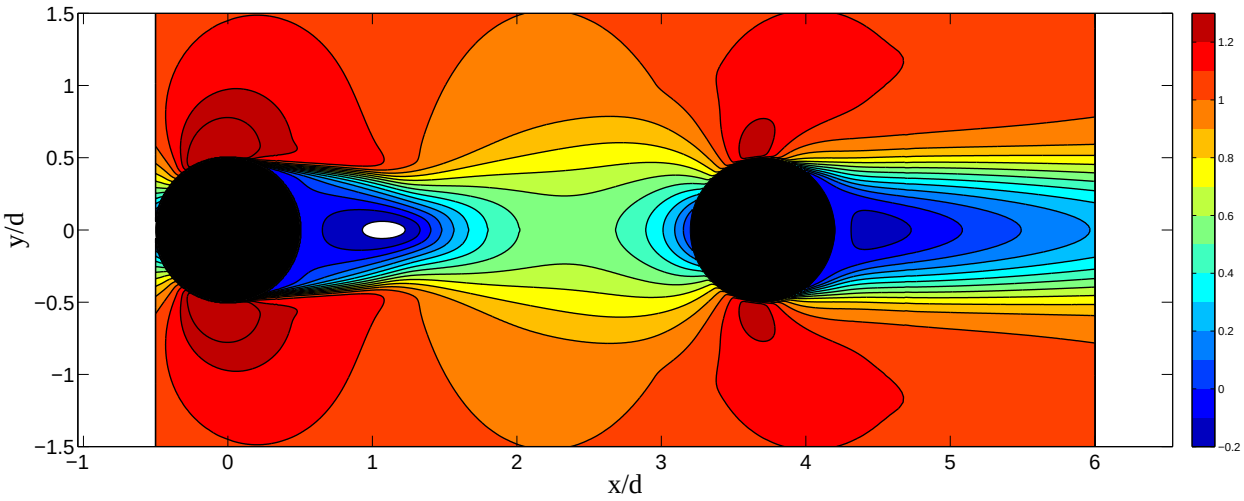

(a) URANS

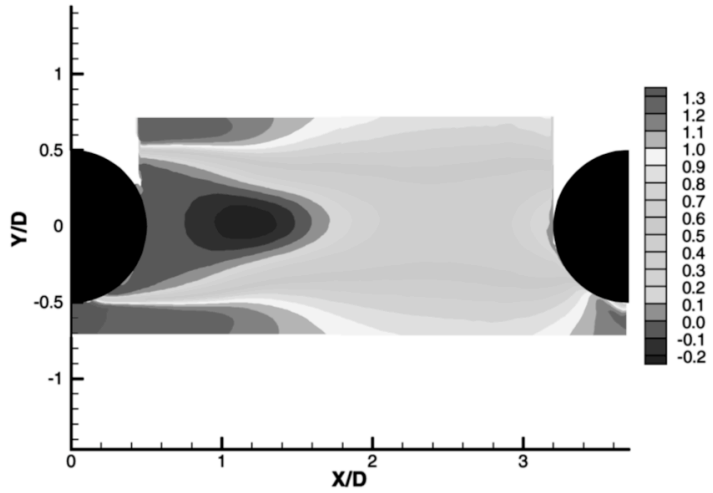

(b) NASA PIV[3]

Figure 4. Mean streamwise velocities (normalised by freestream velocity).

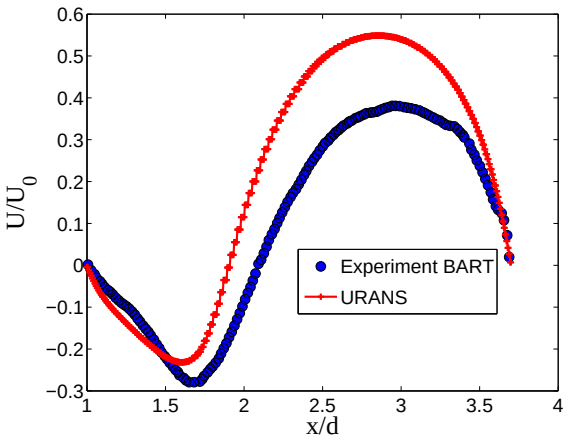

Figure 5. Mean streamwise velocity along centreline between cylinders with $y = 0$. Experimental data from NASA BART facility[2]

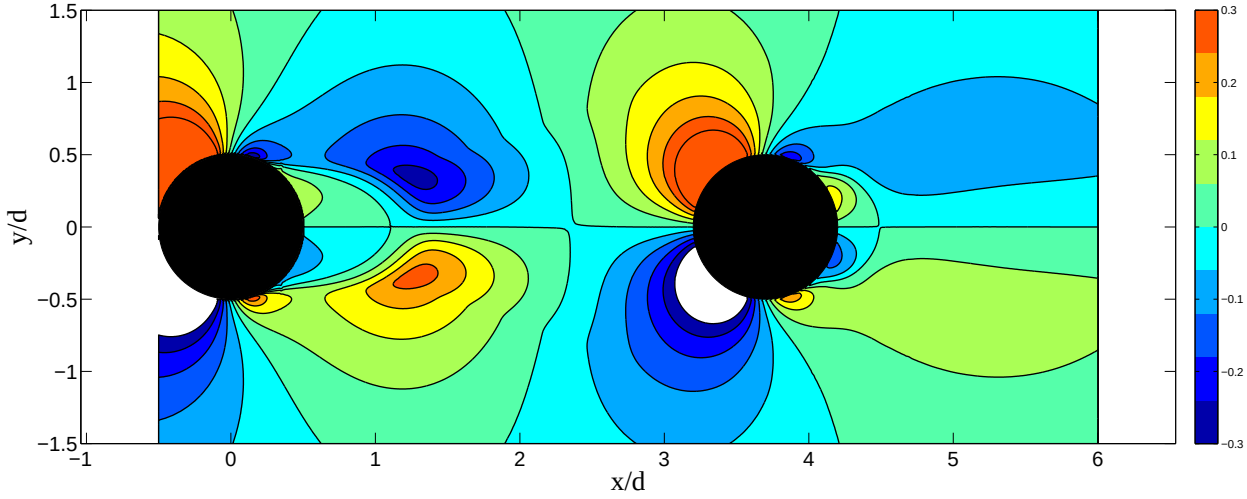

(a) URANS

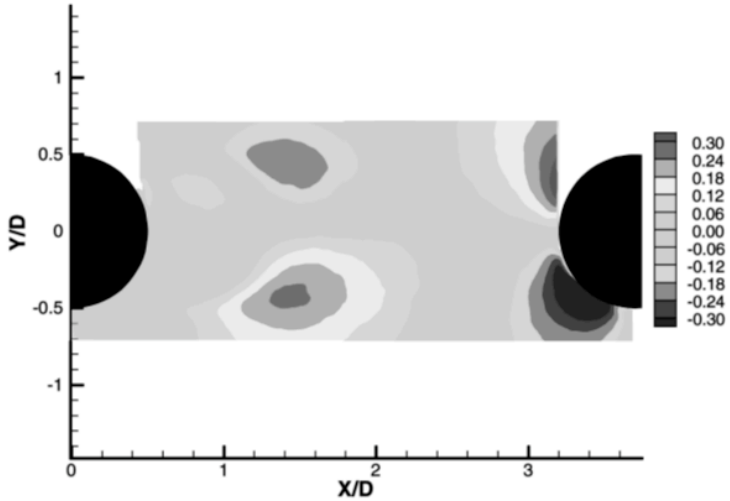

(b) NASA PIV[3]

Figure 6. Mean vertical velocities (normalised by freestream velocity).

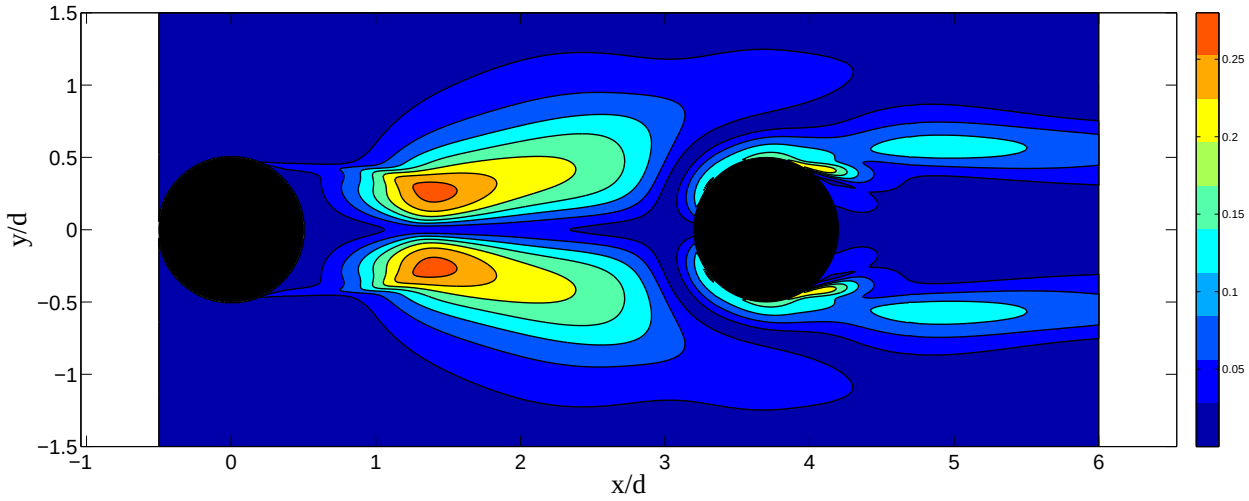

(a) URANS

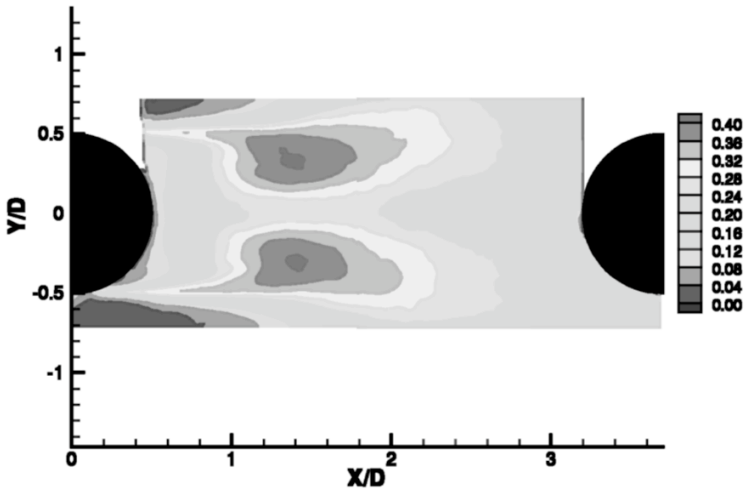

(b) NASA PIV[3]

Figure 7. Time averaged streamwise velocity fluctuation (normalised by freestream velocity).

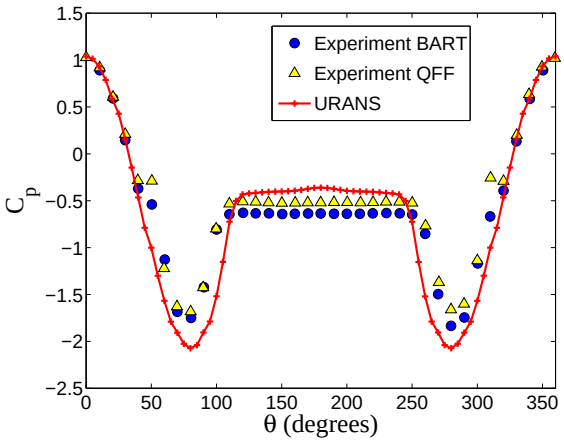

(a) Upstream cylinder

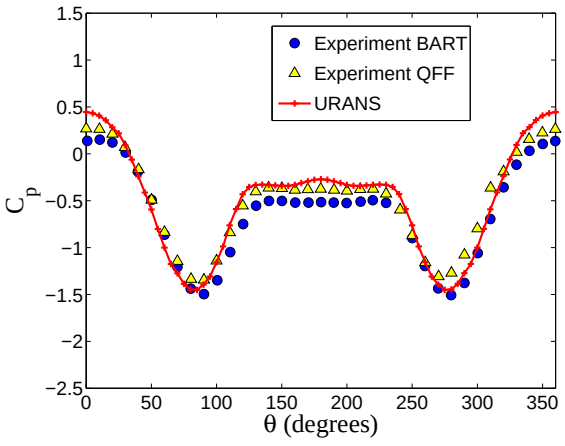

(b) Downstream cylinder

Figure 8. Comparison of computed mean surface pressure coefficient with NASA experimental data.[2]

B. Unsteady Flow

1. *Instantaneous Flowfield*

A comparison between computed and experimental[3] instantaneous spanwise vorticity is shown in Fig. 9. The experimental results show vorticial structures on two scales. As the shear layers form from the separation zones on the cylinder surfaces, Kelvin-Helmholtz (K-H) instabilities create small vortex structures. These eventually influence each other in a pairing process to form larger vortex structures more commonly associated with a von Karman wake. It is interesting and important to note that the larger scale structures consist of well defined smaller vorticial structures that appear to have their origin in the K-H instability that occurs in the earlier shear layer.

The computed vorticity shows only larger scale vorticial structures and they are of the same scale and magnitude of the experiment. The turbulence model used in the URANS simulation does not allow resolution of the fluctuations surrounding the K-H instability and other small scale turbulence effects. This result illustrates why the URANS surface pressures and forces are so tonal in nature. With finer scale structures modelled, only the larger scale, smoothly varying velocity field remains.

2. *Fluctuating Surface Pressure*

A visualisation of the mean-square pressures in the flow about the cylinders is shown in Fig. 10(a). It shows that the most intense surface pressure fluctuations occur about the downstream cylinder. Two regions of intense pressure fluctuation occur in the gap region of the flow, but due to their distance from solid boundaries, make little contribution to the far-field noise.

Root-mean-square (rms) surface pressures are shown for the upstream and downstream cylinders respectively in Figs. 10(b) and (c). The simulation reproduces overall trends but significantly under predicts the peak amplitudes on the upstream cylinder. The comparison is much better for the downstream cylinder and peak fluctuation amplitude matches well with the QFF data. The flow simulations under predict fluctuation amplitude in the base region of the cylinder.

Computed upstream and downstream unsteady surface pressure power spectra at various azimuthal locations are shown in Figs. 11-12 respectively. The computed results are extremely tonal in nature, in contrast to the experimental results. However, the computed results recreate harmonics as seen in the experiments. Additionally, the amplification of some of the first harmonics, as shown in the simulation, was also noticed in the experiments. Note that no temporal decorrelation of the surface pressure signals have been performed on these signals.

The simulations over predict the Strouhal number of the fundamental vortex shedding frequency (St_0). The simulation gives $St_0 = 0.3105$ while it was measured as $St_0 = 0.234$. This is a common problem for two-dimensional URANS simulations and, as discussed earlier, is due to the over prediction of the in-plane Reynolds stress.

3. *Forces*

Simulated unsteady lift and drag coefficients for the upstream and downstream cylinders are shown in Fig. 13. Only the first 50 non-dimensional time units of the data sampling period are reproduced for the sake of clarity. The temporal signals are periodic in nature. The downstream cylinder has a larger fluctuating lift amplitude, compared with the upstream cylinder. This is due to the impingement of the vortex wake generated by the upstream cylinder on the downstream cylinder. The fluctuating drag amplitude on each cylinder also follows the same trend however, the mean drag on the downstream cylinder is lower than the upstream cylinder. The upstream cylinder forms a type of shield in-front of the downstream cylinder, reducing the streamwise velocity impinging upon it and therefore its drag.

Simulated lift and drag power spectra are shown in Fig. 14. For the lift force, Fig. 14(a), a strong tone is predicted at the fundamental vortex shedding frequency, which corresponds to $St_0 = 0.3105$. As mentioned above, the fundamental vortex shedding frequency is over predicted in URANS simulations (experimental measurements give $St_0 = 0.234$). Odd harmonics ($St = nSt_0$ where $n = 3, 5, ...$) of the lift force are recorded on the simulated lift spectra as well. Unsteady surface pressures at $\theta = 90^\circ$ shown in Fig. 12(c) (upper surface, which should be indicative of overall cylinder lift spectra) show all harmonics ($n = 1, 2, 3...$) and suggests that the even harmonics on the cylinder surfaces are out of phase on the upper and lower surfaces.

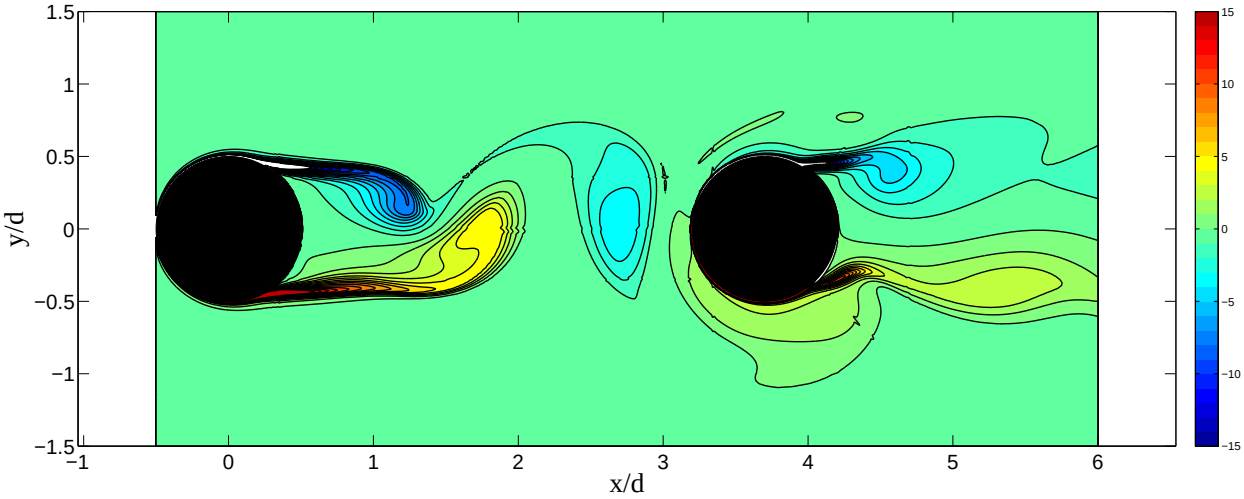

(a) URANS

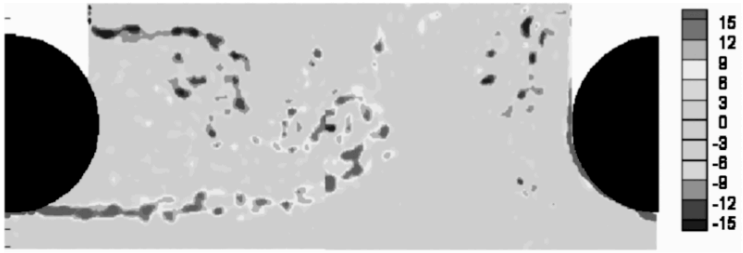

(b) NASA PIV[3]

Figure 9. Instantaneous spanwise vorticity.

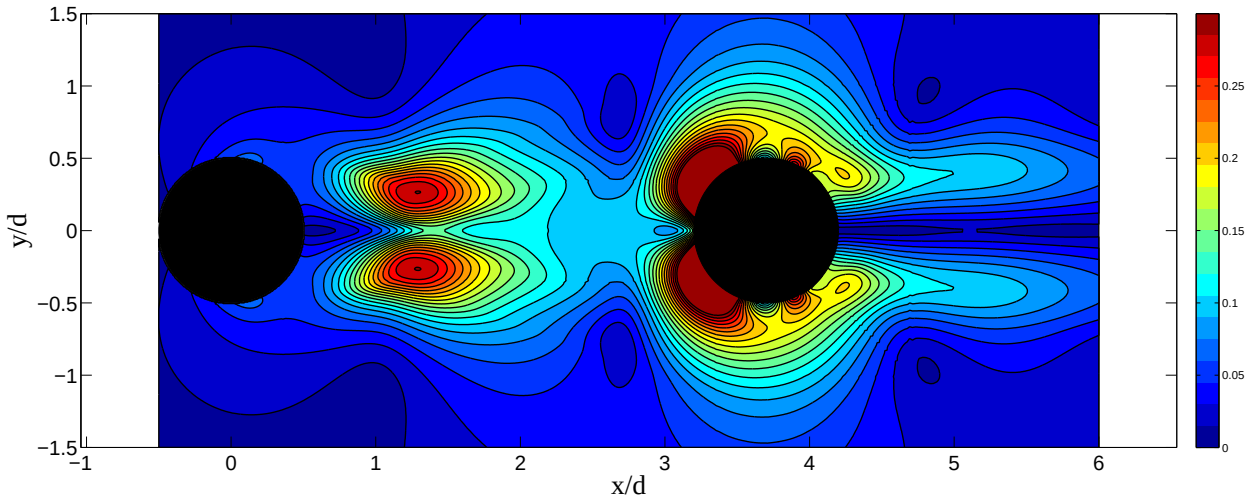

(a) Visualisation

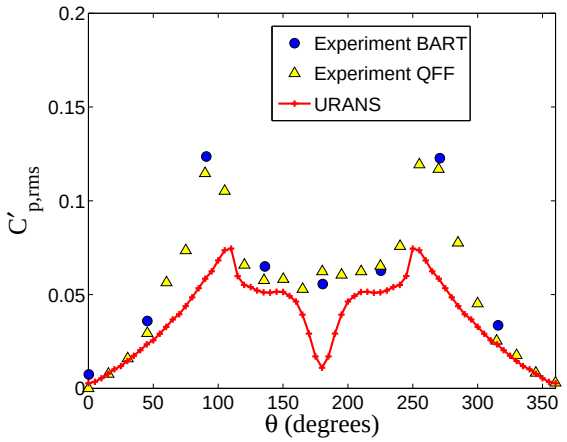

(b) Surface pressure: upstream cylinder

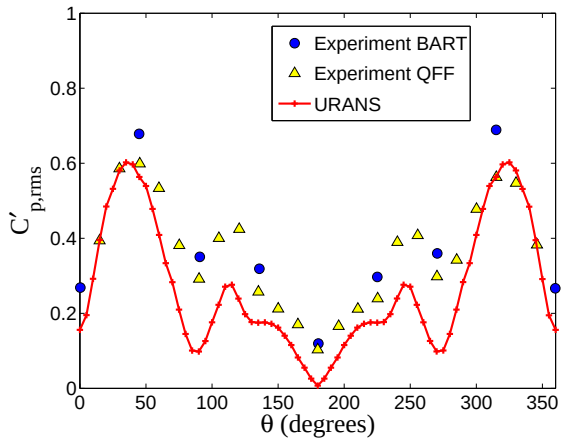

(c) Surface pressure: downstream cylinder

Figure 10. Comparison of computed fluctuating surface pressure coefficient with NASA experimental data.[2]

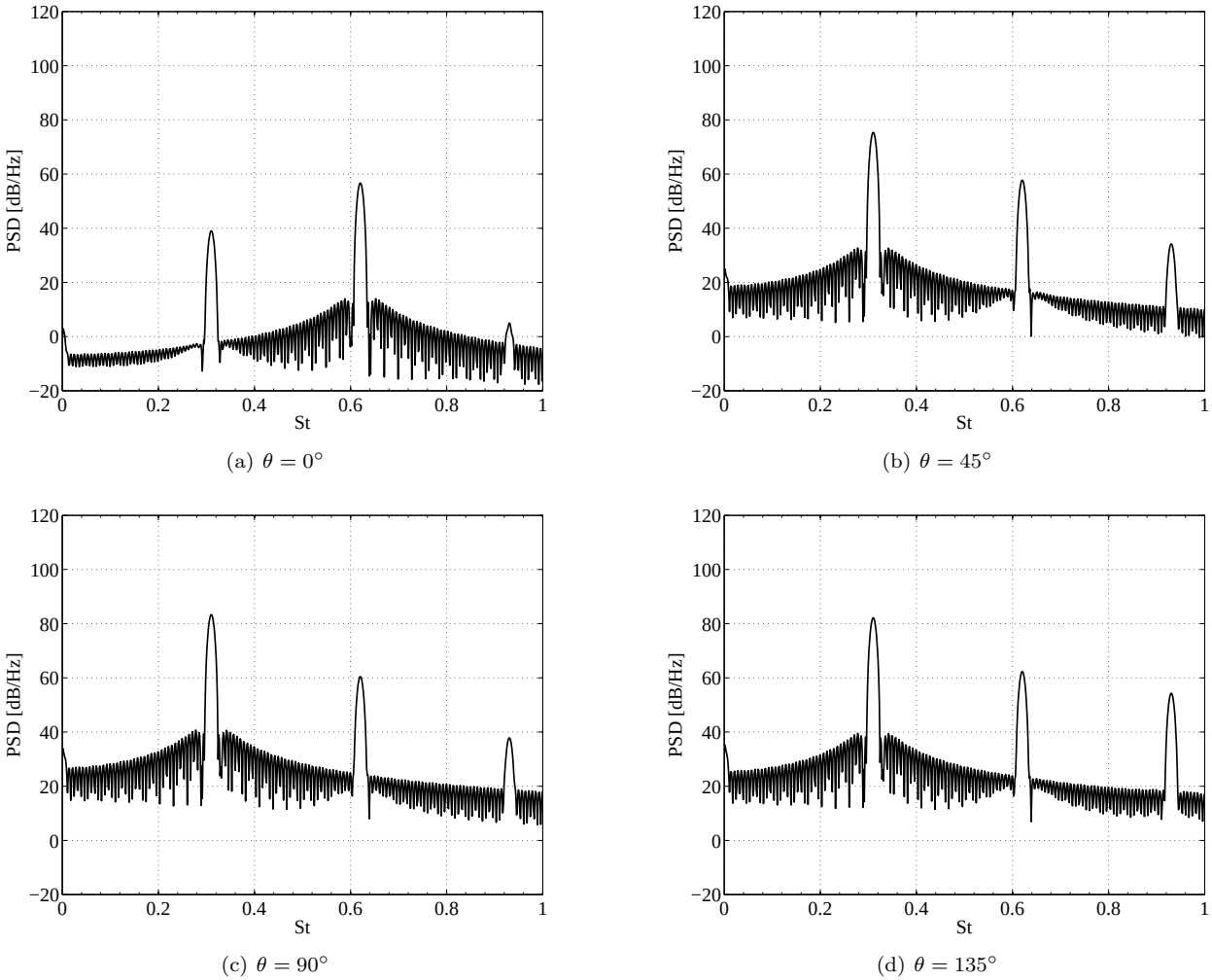

(a) $\theta = 0°$

(b) $\theta = 45°$

(c) $\theta = 90°$

(d) $\theta = 135°$

Figure 11. Computed surface pressure spectra: upstream cylinder.

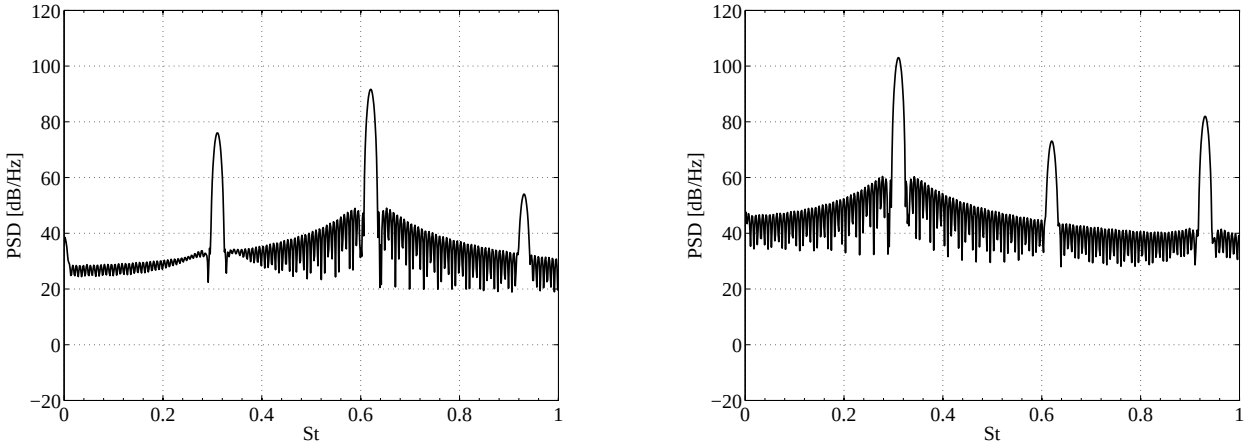

(a) $\theta = 0°$ (b) $\theta = 45°$

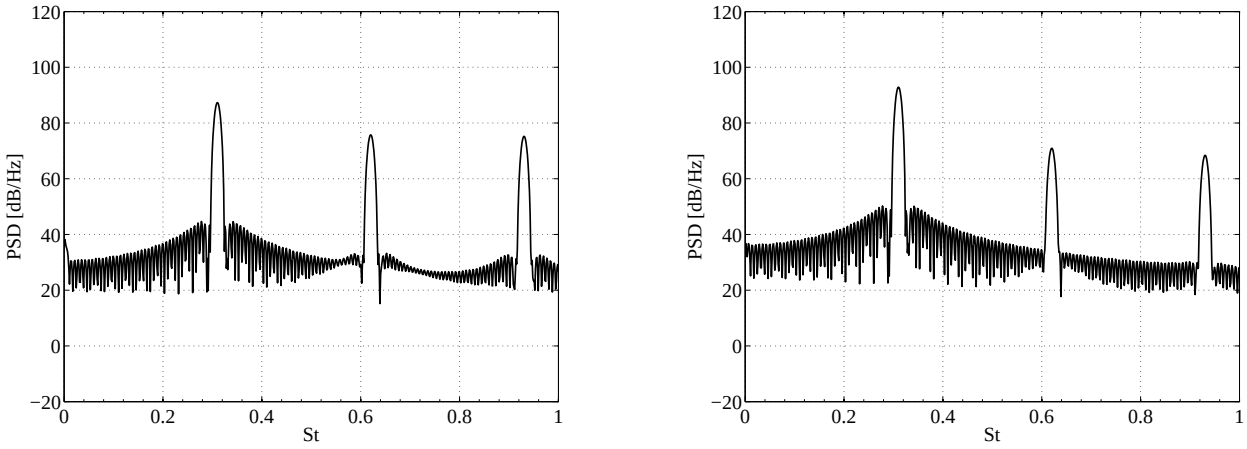

(c) $\theta = 90°$ (d) $\theta = 135°$

Figure 12. Computed surface pressure spectra: downstream cylinder.

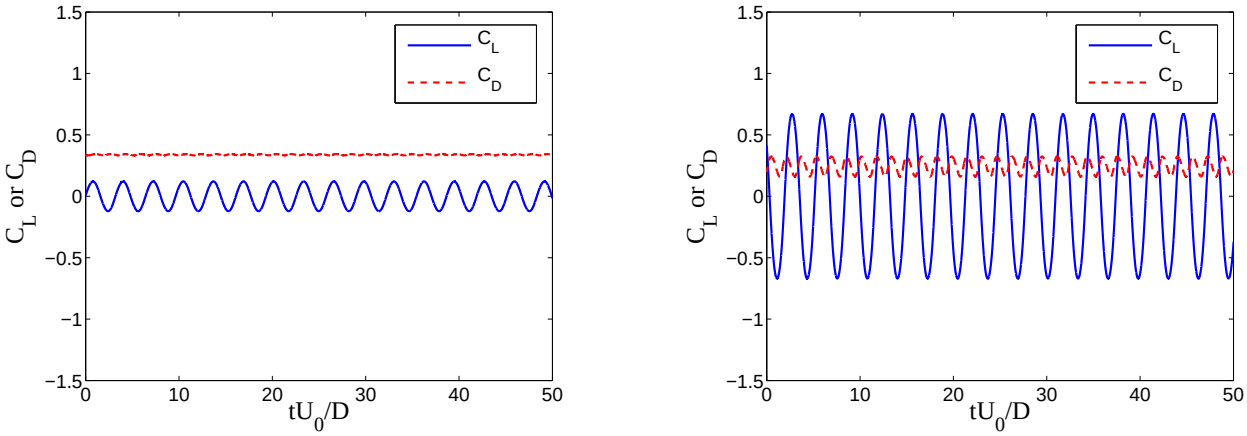

(a) Upstream cylinder (b) Downstream cylinder

Figure 13. Simulated unsteady lift and drag coefficients.

Simulated drag power spectra are shown in Fig. 14(b). The fundamental frequency for the drag spectra is twice that of the lift. This is due to the vortex shedding process as the lift force fluctuates at half the drag frequency. Physically, this is because the shed vortices give the same contribution to drag, but a fluctuation of different sign for the lift on every second cycle. Hence the drag coefficient has peaks at even harmonics of the fundamental Strouhal number ($St = nSt_0$ where $n = 2, 4, ...$). This behaviour also explains the phase relationship of the surface pressures on the cylinder surface.

IV. Acoustic Results

An important part of the acoustic simulation methodology is the estimation of spanwise correlation coefficient. The NASA Tandem Cylinder Experiment[2] provided extensive spanwise surface pressure correlation measurements and these are reproduced in Fig. 15. Statistical models have been fitted to these data for various correlation length scales (L_l). For the present study, a spanwise correlation length scale of $L_l = 0.17$ will be used to estimate far-field noise spectra.

Estimation of the time scale used for temporal decorrelation of the sectional force coefficients (i.e. τ_c) is more difficult. Some guidance can be found in examining experimental unsteady surface pressures records.[15] It is assumed here that disturbances can be expected to occur at about every $N_\tau = 60$ vortex shedding periods. Assuming this is approximately equal to the maximum standard deviation of the time-shift used to decorrelate the signals, $\tau_c \sim \left(\frac{2\pi N_\tau}{St_0}\right)^{-2} \sim 10^{-6}$. This is a crude estimate of the time scale however, as shown below, it produces reasonable results.

The simulated time-domain acoustic pressure is shown in Fig. 16. This result includes the effects of using both temporal and spatial phase dispersion. This result was obtained by using 100 URANS signals with randomly dispersed phase to simulate the temporal decorrelation effects over the time scale $0 \leq \tau \leq 1$. Additionally, spatial decorrelation effects were included by discretising the cylinder into 100 spanwise slices over the range $0 \leq \eta \leq 1$. As shown in the figure, the statistical models provide considerable variation in the time-domain signal. The acoustic power of the signal was scaled so that it is identical to the acoustic power of the signal obtained using unmodified URANS simulated force data.

Figure 17 compares simulated far-field noise with experimental measurements taken in the QFF at the locations of microphones A, B and C.[2] Table 2 lists the microphone locations with respect to the center of the upstream cylinder. The positions of the microphones corresponds to approximately one wavelength at the fundamental shedding tone. As discussed above, near field effects are negligible for the frequency range of interest. The numerical results were resampled at 8.882 kHz ($St = 11.7$) in order to reduce the size of the numerical data record and make it more managable. During spectral analysis the data was processed using a Hamming windowing function so that the frequency resolution was $\Delta f = 3.125$ Hz (identical to experiment). The spectra were calculated by obtaining the power spectral density of 100 separately simulated acoustic signals of the type shown in Fig. 16 and averaging them.

Table 2. Simulated microphone positions (with respect to the centre of the upstream cylinder).

Name	x/d	y/d
Microphone A	-8.33	27.817
Microphone B	9.11	32.49
Microphone C	26.55	27.815

The simulated results show excellent agreement with experiment around the main tone. Broadband contributions are generally predicted well however, the simulation over predicts the acoustic level when $St > 1$. Peak simulated levels at the harmonics are too high when compared with experiment. The observed differences can be attributed to an over prediction of the harmonic force components by the URANS simulations.

It is interesting to observe the magnitudes of the harmonics for microphones A and C, compared with microphone B. Microphones A and C are upstream and downstream of the cylinders, respectively, while microphone B is nearly above them. The larger angle from the vertical of microphones A and C means that the drag dipoles of each cylinder are responsible for more of the acoustic signals than for microphone B.

This is observed in Fig. 17, where the strength of the drag tone and its harmonics are more pronounced for microphones A and C in both the numerical and experimental spectra. The extremely tonal nature of the URANS signals at the higher harmonics are not broadened by the statistical method. More work is required to understand why this is the case and to develop better statistical modelling procedures.

V. Conclusion

A two-dimensional URANS simulation of the NASA tandem cylinder experiment was performed using the OpenFOAM software package. Mean and unsteady aerodynamic data were compared with experimental results. In general, the URANS simulation provided reasonably accurate reproduction of experimental flow measurements. The deviations that were observed relate to the two-dimensional nature of the simulations and the restrictions this places on adequately recreating the flow physics.

A compact form of Curle's theory was used to simulate the acoustic results using the two-dimensional URANS force data as an input. In order to improve the accuracy of the acoustic computation, statistical models were used in an attempt to insert statistically realistic three-dimensional flow effects into the time-domain acoustic record. A spanwise model (based on the method of Casalino and Jacob[12]) was used and a new temporal model was presented and used to include random time-based effects seen on experimental surface pressure records. Upper and lower frequency limits for the method were obtained using arguments based on acoustic compactness and near-field effects, respectively. The acoustic simulation method provides good overall agreement with experimental acoustic power spectra measurements obtained from NASA's Quiet Flow Facility (QFF) for the NASA Tandem Cylinder Experiment. Further development is required to improve spectral broadening of harmonic components for $St \geq 2St_0$.

References

[1]Zdravkovich, M., "Review of flow interference between two circular cylinders in various arrangements," *ASME Journal of Fluids Engineering*, Vol. 99, 1987, pp. 618–631.

[2]Lockard, D., Khorrami, M., and Choudhari, M., "Tandem Cylinder Noise Predictions," *Paper No. AIAA 2007-3450*, 13 th AIAA/CEAS Aeroacoustics Conference, 2007.

[3]Khorrami, M. R., Choudhari, M. M., Lockard, D. P., Jenkins, L. N., and McGinley, C. B., "Unsteady Flowfield Around Tandem Cylinders as Prototype Component Interaction in Airframe Noise," *AIAA Journal*, Vol. 45, No. 8, 2007, pp. 1930–1941.

[4]Jenkins, L., Neuhart, D., McGinley, C., and Choudhari, M., "Measurements of Unsteady Wake Interference Between Tandem Cylinders," *Paper No. AIAA-2006-3202*, 36th AIAA Fluid Dynamics Conference and Exhibit, 2006.

[5]Hutcheson, F. and Brooks, T., "Noise Radiation from Single and Multiple Rod Configurations," *Paper No. 2006-2629*, 12 th AIAA/CEAS Aeroacoustics Conference, 2006.

[6]Leclercq, D. and Doolan, C., "The Interaction of a Bluff Body with a Vortex Wake," *Journal of Fluids and Structures (Accepted 7/3/09)*, Vol. 25, No. 5, 2009.

[7]Inoue, O., Mori, M., and Hatakeyama, N., "Aeolian tones radiated from flow past two square cylinders in tandem," *Physics of Fluids*, Vol. 18, No. 4, Jan 2006, pp. 046101.

[8]Lockard, D. P., Choudhari, M. M., Khorrami, M. R., Neuhart, D. H., Hutcheson, F. V., Brooks, T. F., and Stead, D. J., "Aeroacoustic Simulations of Tandem Cylinders with Subcritical Spacing," *Paper No. AIAA-2008-2862*, 14th AIAA/CEAS Aeroacoustics Conference, 2008.

[9]Casalino, D., Jacob, M., and Roger, M., "Prediction of rod-airfoil interaction noise using the FW-H analogy," *AIAA Journal*, Vol. 41, No. 2, Feb 2003, pp. 182–191.

[10]Weller, H., Tabor, G., Jasak, H., and Fureby, C., "A Tensorial Approach to CFD using Object Orientated Techniques," *Computers in Physics*, Vol. 12, No. 6, 1998, pp. 620–631.

[11]OpenCFD, "OpenFOAM: The Open Source CFD Toolbox," http://www.opencfd.co.uk/openfoam/, 2007.

[12]Casalino, D. and Jacob, M., "Prediction of aerodynamic noise from circular rods via spanwise statistical modelling," *Journal of Sound and Vibration*, Vol. 262, 2003, pp. 815–844.

[13]Curle, N., "The influence of solid boundaries on aerodynamic sound," *Proc. Roy. Soc. London*, Vol. A231, 1955, pp. 505–514.

[14]Roshko, A., "Perspectives on Bluff Body Aerodynamics," *Journal of Wind Engineering and Industrial Aerodynamics*, Vol. 49, 1993, pp. 79–100.

[15]Norberg, C., "Fluctuating lift on a circular cylinder: review and new measurements," *Journal of Fluids and Structures*, Vol. 17, 2003, pp. 57–96.

[16]Rajagopalan, S. and Antonia, R., "Flow around a circular cylinder—structure of the near wake shear layer," *Experiments in Fluids*, Vol. 38, 2005, pp. 393–402.

[17]Kim, S., "Large Eddy Simulation of Turbulent Flow Past a Circular Cylinder in Subcritical Regime," *Proceedings of the 44th AIAA Aerospace Sciences Meeting and Exhibit*, No. AIAA-2006-1418, Reno Nevada, 2002.

[18]Dowling, A. and Ffowcs-Williams, J., *Sound and Sources of Sound*, John Wiley and Sons, 1983.

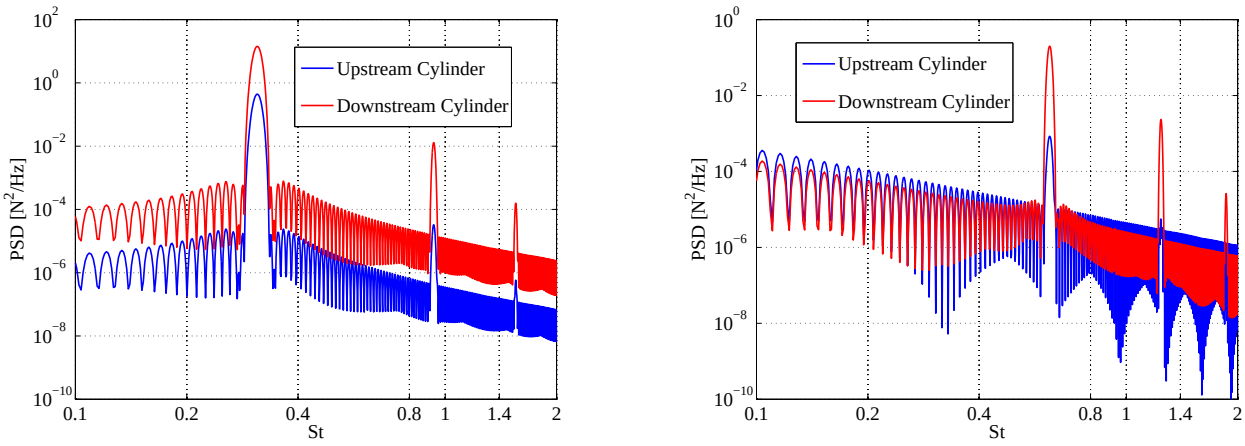

(a) Lift (b) Drag

Figure 14. Simulated unsteady force power spectra.

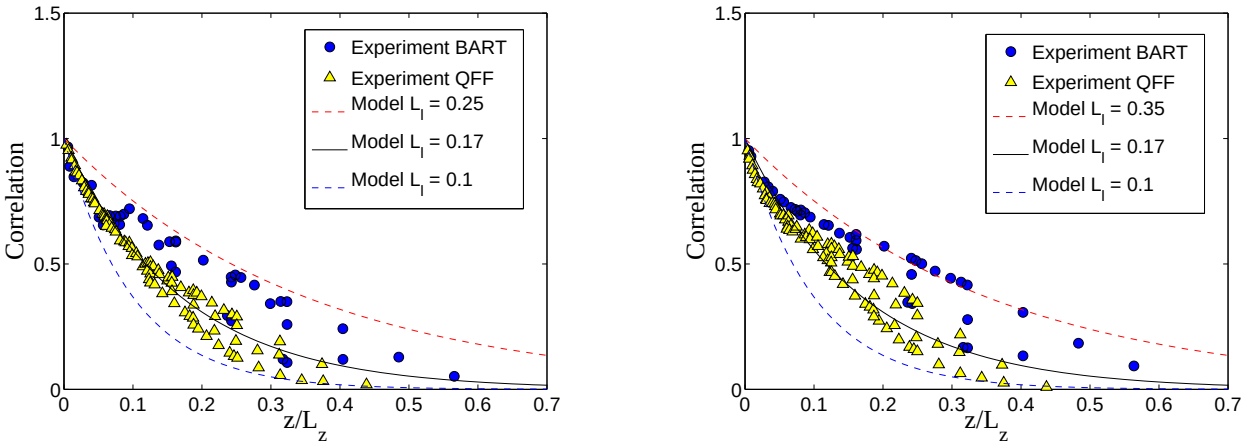

(a) Upstream cylinder (b) Downstream cylinder

Figure 15. Correlations computed from experimental surface pressures[2] and fitted spanwise correlation model.

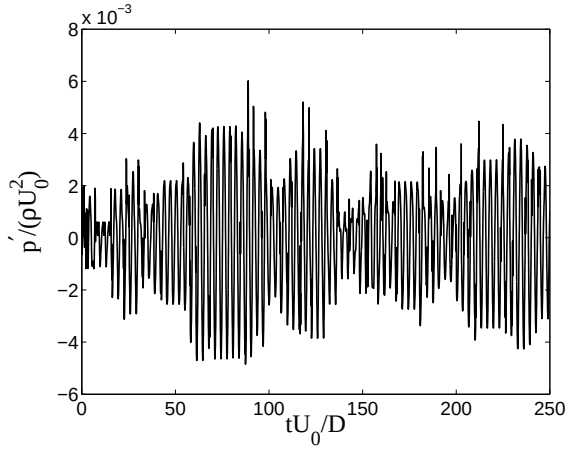

Figure 16. Simulated acoustic pressure at Microphone B.

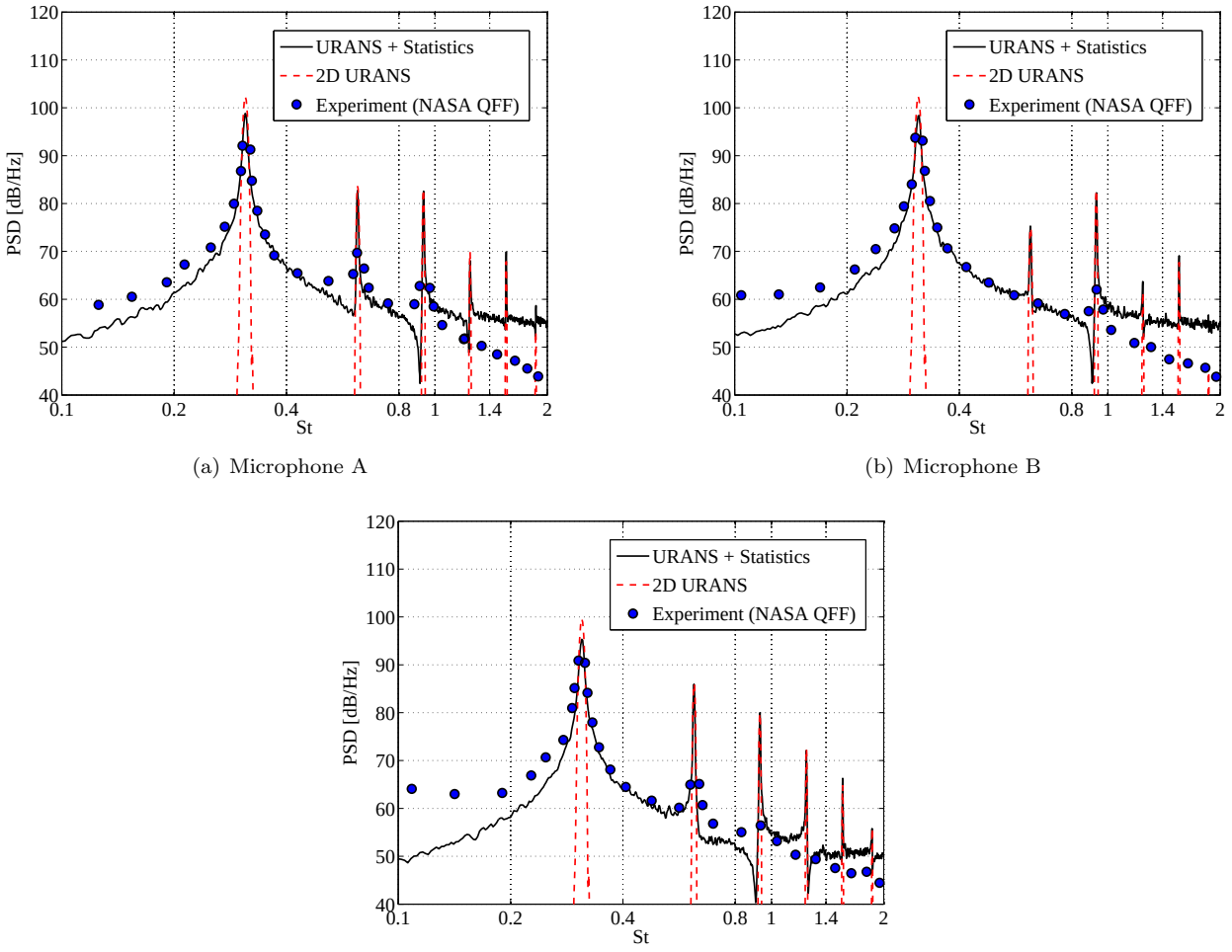

(a) Microphone A

(b) Microphone B

(c) Microphone C

Figure 17. Comparion of simulated and experimental acoustic results for Microphones A, B and C. Experiments obtained in NASA's Quiet Flow Facility (QFF).[2]